Calibration of the insert/tool holder thermal contact resistance in stationary 3D turning

Alexandre Mondelin, Frédéric Valiorgue, Eric Feulvarch, Joël Rech, Michel Coret

Calibration of the insert/tool holder thermal contact resistance in stationary 3D turning

Alexandre Mondelin [a,b], Frédéric Valiorgue [a], Eric Feulvarch [a], Joël Rech [a], Michel Coret [b] [a]

University of Lyon, LTDS/ENISE, 58 Rue Jean Parot, 42023 Saint Etienne, RA, France
[b] *University of Lyon, INSA/LaMCoS, UMR CNRS 5259, 27 Avenue Jean Capelle, 69621 Villeurbanne, France*

- ► Estimation of the insert/shim/tool-holder thermal contact resistance (RTC).
- ► Calibration procedure of thermal contact resistance based on laser heating.
- ► 3D numerical model of turning device used for inverse method of RTC quantification.
- ► Sensitivity study of the RTC value impact on heat discharge during turning.

Keywords:
Turning
Thermal contact resistance
Laser heating
Heat flux identification

Modeling machining processes, especially turning, is the subject of a large number of studies today. The objective is to optimize cutting conditions and improve tool lifetime as well as the quality of the pieces produced. However studying various phenomena such as tool wear requires simulating very long machining times in order to reach the stabilized state, among other things. These stationary simulations require a very good calibration of the limit conditions representing the experimental reality. In particular, the thermal contact resistance of the insert/tool-holder body contact plays a very significant part in removing the heat generated. The aim of this article is to propose an experiment/simulation procedure to calibrate this resistance. Based on laser heating and temperature measurement, a numerical sensitivity study has made it possible to estimate the value of this resistance in the case of a non-coated insert and a carbide body.

1. Introduction

Turning is the most common material removal machining process. The tools are made of tool holders and inserts cutting the material. During the cutting operation, three shearing areas appear. A primary shearing area extends from the tool cutting edge to the chip root. A secondary shearing area corresponds to the friction of the chip on the cutting face and a tertiary shearing area appears on the flank surface where the insert "rubs" the machined surface on account of spring-back essentially. Those areas are the object of severe heating due to the material plastic dissipation [1]. It is commonly admitted that most of the heat generated is removed by the chip, but the fraction of the remaining heat (approximately 8–10%) is dissipated by the tool and the piece [2]. Despite the low proportion of heat evacuated by the tool and the piece, the temperatures may rise above 1000 °C as they are applied on very concentrated areas. As a matter of fact, although the powers are a few tens of Watts, the flux densities reach several hundreds of Watts per squared millimeter [3]. The temperature levels reached create three major problems that impact adversely tool productivity and the quality of the pieces machined: tool wear [4], deterioration of the pieces surface integrity as well as their geometrical tolerances [5]. It can be seen that a good understanding and control of the heat generation processes during cutting are at the forefront of current research activities aimed at improving both productivity and the quality of the pieces manufactured. Those activities are often addressed both from the experimental and numerical modeling points of view.

With regard to experiments, various techniques have been described in the literature to measure temperatures. They are essentially based on infrared thermography and thermocouples. In

1961, Boothroyd used infrared films to map temperature fields under stationary conditions [6]. On the other hand, Chao et al. used photosensitive Pbs cells to measure temperatures on cutting tool flank surfaces [7]. Prins used a pyrometer to measure temperatures on the cutting surface [8]. Using thermocouples inserted into the tool, Basti [9] measures temperatures on the cutting surface during turning (unmoving tool). Le Coz et al. [10] have developed an acquisition system to measure temperature of rotating cutting tools (drilling or milling). Besides, various studies used the thermal imaging camera to shoot the cutting scenes and extract representative temperature fields during longitudinal turning [11] or orthogonal cutting process [12] for example. It can be seen that all these experimental techniques are operational but do not make it possible to access the very heart of heat generation and transfer phenomena. However the interest of these approaches lies in the fact that they provide the data needed to validate simulations that make it possible to gain access to physical quantities difficult to measure in the cutting area. For example, based on these experimental data, inverse methods may be used to estimate the moving heat source in machining process [13].

With regard to numerical modeling, turning simulations fall into two categories: the Lagrangian approach [14] and the Arbitrary Lagrangian Eulerian (ALE) approach. The Lagrangian approach consists in imposing a similar movement to the material and the mesh [15]. This makes it possible to simulate chip and shearing zone forming and predict cutting stresses in the early moments of machining [16].

ALE approaches are based on the use of a mesh partially independent from the material movement [17]. This type of simulation makes it possible to reproduce a more realistic flow around the nose radius [18] and thus obtain realistic heat sources [19].

Generally speaking, machining thermo-mechanical simulations are aimed at simulating the whole cutting operation, i.e. the material separation around the nose radius, the shearing areas as well as heat generation and propagation within the piece, the chip and the tool. Unfortunately these simulations are very demanding and with current computation methods it is difficult to simulate more than a few machining milliseconds. Under these conditions, it is impossible to reach the mechanical, let alone thermal, stationary condition. There is not enough time for heat transfer phenomena to reach the shim and tool-holder. However there is a solution consisting in extracting thermal loadings to make a thermal simulation only under a stationary condition. In this way it is possible to obtain thermal results representative of a continuous machining operation [20]. In this configuration, temperatures rise in the shim and tool-holder. It is therefore necessary to have a very good knowledge of the thermal contact resistances (RTC) on the interfaces and particularly the insert/shim contact resistance which is the subject of this study.

The thermal contact resistance (RTC) between two static flat surfaces is sometimes difficult to accept. At a microscopic point of view (roughness scale), Grzesik [21] especially considered that contact could be partially heterogenous, leading to the formation of a RTC. This idea is also developed by Courbon et al. [22] for the tool-chip interface. Courbon et al. [22] explains that the real contact area can be limited at a certain scale by the imperfections of the surfaces in contact. This leads to consider a RTC at a macroscopic point of view.

Regarding the calibration of the RTC, different experimental devices have been developed. On one hand, some authors estimate the RTC recreating the process itself. B. Bourouga et al. [23] and Abdulhay et al. [24] fine-tunes the RTC value measuring the temperature and the heat flux during the stamping of an aluminum cylindrical part on a waspalloy tool. Results vary from 1 to 50,000 mm^2 K/W depending on the real contact area (at a microscopic scale). Using thermocouples, Abdul Hay et al. [25] estimate the heat flux between tool and blank. Then, knowing the two surface temperatures on the blank and the tool sides as well as the flux density at the contact interface, they estimate the RTC value (varying from 200 to 2000 mm^2 K/W during stamping of boron-alloyed steel at 930 °C under high pressure). On the other hand, experimental devices dedicated to RTC calibration are developed. For example Rogeon et al. [26] and Rosochowska et al. [27] use cylindrical samplings identical to the considered interface materials. Heat flux through the sampling stack is created using heating devices and thermocouples that allow controlling boundary conditions. RTC is easily estimated by comparing the temperature on each side of the samplings. These devices could be mounted on compression test machine to reproduce process condition of pressure [26].

Very few studies have been conducted so far on tool-holder/shim/insert interface thermal modeling. In Abukhshim et al. [28]'s study the tool-holder/shim/insert interfaces are assumed to be perfect whereas Carvalho et al. [29] evaluate the contact resistances from the properties of an air blade present inside the interfaces. It is important to note that Carvalho et al. [29] admits that his approach is not validated and may cause errors in the simulations. Within this framework, the aim of this article is to propose an experiment/simulation procedure to calibrate the contact resistance between the insert and tool-holder body via laser heating of the insert. The interest of this approach lies in the fact that it makes it possible to gain access to the data required to perform simulations under the stationary condition of a machining operation.

This approach can be developed as follows: with the assumption that we have knowledge of the material thermal properties, the laser beam diameter and the coefficient of convection exchange with the air, the laser heating power actually absorbed is calibrated first. To do so, the insert alone (without shim or tool holder) is heated by a laser beam. Thus the actual heating power is calibrated by comparing experimental and simulated temperatures. From the laser flux thus calibrated, the next step evaluates the thermal contact resistance at the tool-holder insert/shim interface by laser heating of the tool-holder/shim/insert set and comparison with the simulations performed. Finally the last step is the validation of the resistance value obtained under thermal conditions different from those used for the calibration process. This is done by comparing the temperatures simulated and measured based on pulsed laser heating or long term cycles.

In the present article, the whole procedure is described into three parts. The first one is the presentation of the whole experimental set-up (in its various configurations) as well as the numerical tool used to calibrate those data. The second one presents successively the laser flux and contact resistance calibration. Finally the last part validates the results obtained by applying laser heating cycles different from those used for calibration.

2. Experimental devices

Heating trials have been done using a continued Laser Nd-YAG Trumpf HL2006D ($\lambda = 1064$ μm). The laser is power-controlled to obtain 70 W at the exit of the focusing lens (Fig. 1a).

Non-coated carbide inserts (6% Co-94%WC) have been used. The insert geometry is TCMW1608: triangle form; clearance angle = 7°; cutting edge length = 16 mm; nose radius = 0.8 mm; without a chip-breaker (plane faces).

The tool-holder designation is STFC L2020 K16. It is composed of a steel body and a carbide shim. In order to focus the study on the thermal resistance between the insert and the rest of the tool-holder, the carbide shim has been stuck on the tool-holder steel

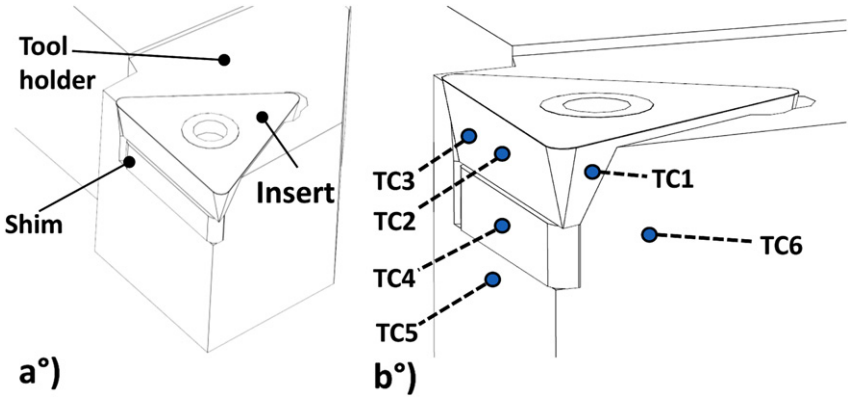

Fig. 1. Turning device and locations of thermocouples.

body using heat conductive metallic glue. These different parts of the turning device are presented Fig. 1.

The temperatures were measured on accessible locations of the insert, the shim and the tool-holder by using a type K thermocouple and a Frontacq data acquisition system with a PC-controlled voltmeter. The acquisition frequency is fixed at 100 Hz. Fig. 1b presents the locations of thermocouples (TC). Using the described acquisition device, the uncertainty of temperature

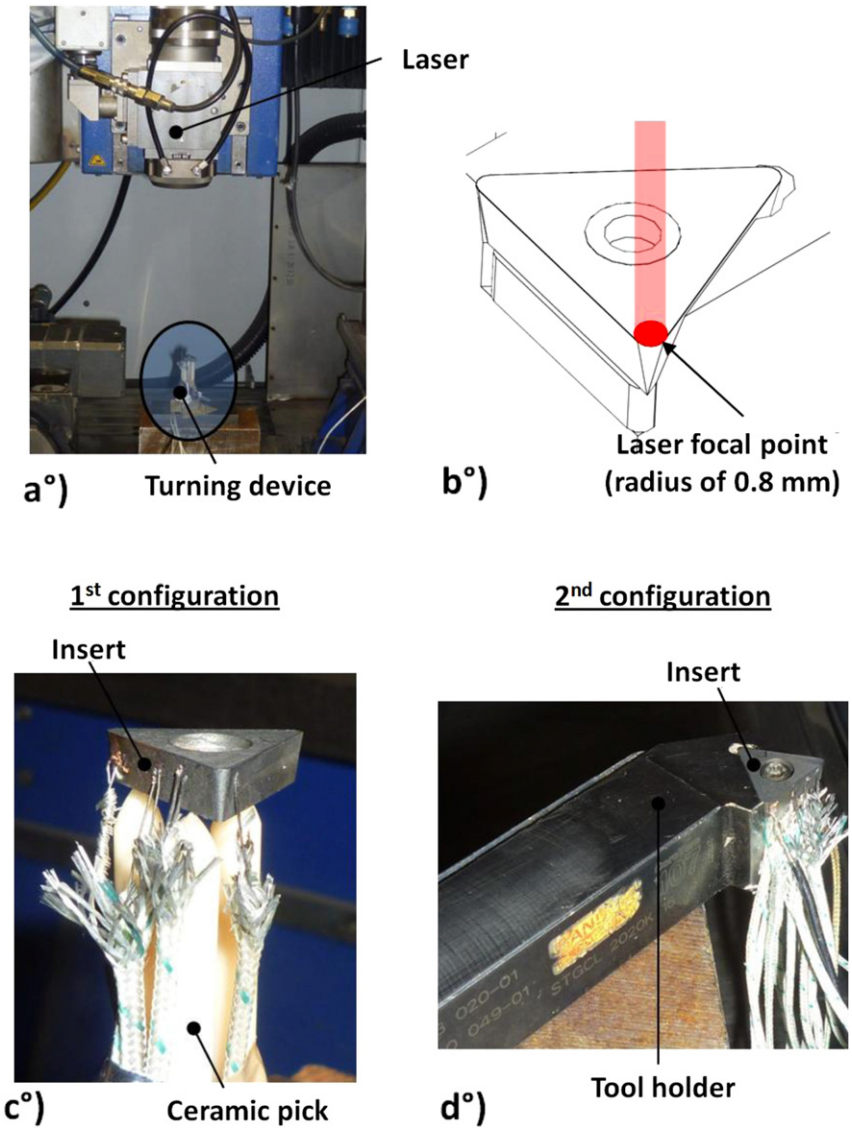

Fig. 2. Experimental device and heating configuration for the two calibration steps.

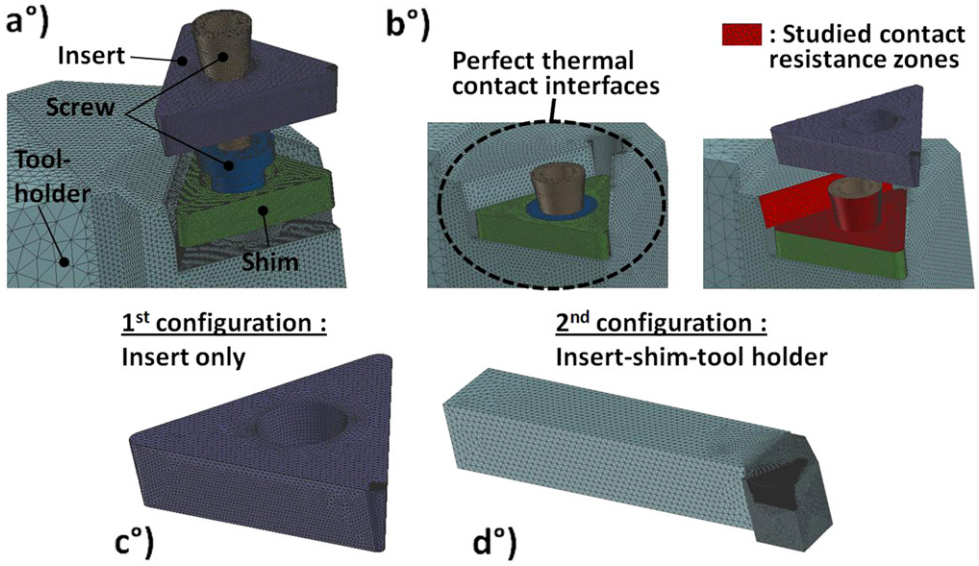

Fig. 3. Numerical model used for the calibration step.

measurement, could be estimated at 0.3% of the measured temperature. In the range of 200–400 °C, the uncertainty is then about 0.6–1.2 °C.

The laser beam has been focused to obtain a beam radius of 0.8 mm (so equal to the nose radius). The rake face of the insert has been placed below the laser, perpendicularly to the beam. The focal point is positioned at the nose center of the insert (Fig. 2b). This nearly corresponds to the tool-chip contact zone.

To calibrate the actual penetrating laser flux and the thermal contact resistances, two configurations are used.

Firstly, the insert alone is heated. It is placed on three ceramic picks in order to avoid thermal conduction (Fig. 2c). The only thermal exchange considered is convection with the air. Thermocouples 1, 2 and 3 are used.

Secondly, the insert is fixed on the tool-holder. So, heat exchanges occur by conduction between the insert, the shim and the tool-holder body (Fig. 2d). All thermocouples are considered.

3. Numerical model used for the calibration step

To calibrate the actual laser flux power and the thermal contact resistance between the insert and the tool-holder, a numerical model of the laser heating experiments is used. The 3D Finite Element model is composed of linear tetrahedron elements.

The insert consists of 137,955 elements, the shim of 122,103 elements and the tool-holder of 622,150 elements. The other parts (two concentric fixing screws) represent 105,772 elements (Fig. 3a). The grid size has been adapted in order to limit the influence of the mesh size on the results. Thus, in the area with the highest temperature gradient (insert nose), the average size of the elements is 0.05 mm. Then this value gradually increases up to 2 mm at the extremity of the tool-holder.

For time integration, the model uses an implicit backward Euler algorithm [30] and the time step is constant and equal to 0.02 s. The convergence criterion is set at 10^{-2} W.

The laser flux is modeled by surface heat flux density. The applied heat flux has a constant value on disk with a radius of 0.8 mm (comparable to the laser beam). The thermal contact resistance is modeled by the Equation (1):

$$\varphi = \frac{\Delta\theta}{R} \tag{1}$$

where φ is the heat flux density in W/mm^2, $\Delta\theta$ is the temperature difference in °C and R the thermal contact resistance in mm^2 °C/W.

Given that the shim is stuck on the tool-holder using conductive metallic glue, the shim/tool-holder contact will be assumed to be perfect in the simulations (null contact resistance). The same applies to minor screw/shim and screw/tool-holder contacts. The whole set-up has therefore perfect thermal contacts.

The resistance we are calibrating is applied to all the boundaries of the insert in contact with the shim (essentially) but also with the tool-holder and the screw (Fig. 3b).

The convection heat transfer coefficient with the air is fixed at $h = 40 \times 10^{-6}$ W/mm^2/°C for external boundaries of the different parts. The heat exchange with the external medium is governed at each node by the Equation (2):

$$\varphi_{conv} = h \cdot \Delta\theta \tag{2}$$

where φ_{conv} is the heat flux density in W/mm^2, $\Delta\theta$ is the temperature difference between the modeled parts and the external medium in °C and h is the convection heat transfer coefficient W/mm^2/°C.

The ambient temperature is considered to be equal to 23.5 °C in the numerical model (according to the value observed during the

Table 1
Properties of the WC carbide (H13A).

Insert and shim: WC carbide (H13A) [31,32]			
Temperature [°C]	Density [kg m^{-3}]	Heat capacity [J °C^{-1}]	Thermal conductivity [W m^{-1} °C^{-1}]
20	14,830	220	110
100	14,830	244	105
300	14,830	290	98
500	14,830	320	90
700	14,830	328	82
900	14,830	337	75

Table 2
Properties of high speed steel.

Tool-holder and screw: high speed steel [33,34]			
Temperature [°C]	Density [kg m^{-3}]	Heat capacity [J °C^{-1}]	Thermal conductivity [W m^{-1} °C^{-1}]
20	7820	500	50
100	7820	533	45
300	7820	613	40
500	7820	700	36
700	7820	714	31
900	7820	720	23

experiments). The following material thermal properties are considered (Table 1 [31,32] and Table 2 [33,34]):

In order to compare numerical and experimental temperature results, the locations of thermocouples have been accurately measured on the experimental device (Fig. 4) using welding marks. Then, corresponding nodes on the numerical model have been located. So, each thermocouple temperature measurement is compared with the average temperature value of a set of matching nodes.

4. Calibration procedure

4.1. Laser heating test

The heating cycle chosen for laser flux and thermal resistance calibration is presented in Fig. 5. The heating phase is three seconds long, and then the cooling phase is free.

Fig. 6 presents temperature measurements of thermocouples 1, 2 and 3 for the two configurations:

- Fig. 6a: heating of insert alone
- Fig. 6b: heating of insert fixed on the tool-holder

When comparing the temperature curves in the two experimental configurations, the differences are significant. Firstly, the maximum temperature reached is 285 °C for the insert alone and only 245 °C for the set. The cooling phase is also dissimilar. The cooling rate is clearly higher for the assembly. Of course all these differences are directly attributable to the presence (or absence) of heat transfer between the insert and tool-holder body. Then, it is already possible to note that the thermal behavior of an insert alone is totally different from the 'insert + tool-holder' set (even if the heating phase only lasts three seconds).

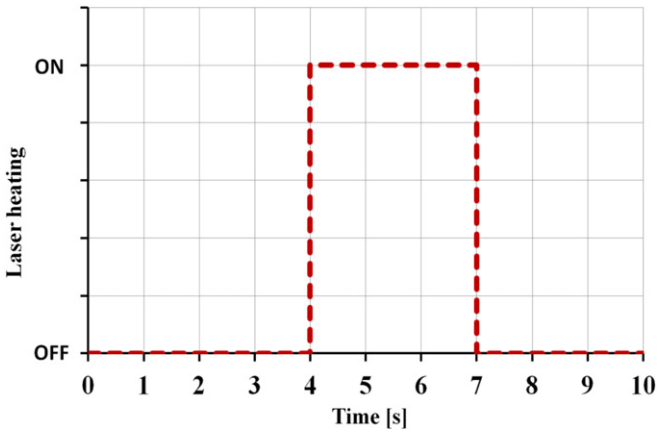

Fig. 5. Heating cycle of three seconds used for the calibration step.

4.2. Calibration of the actual laser flux power

In this first calibration step, the aim is to know the actual laser flux power. Even if it is possible to globally control the laser power (fixed at 70 W in our study), it is very difficult to know the flux power which really penetrates the carbide insert and contributes to the heating of the material. Indeed, there are power losses in the optical system and by reflection at the surface of the insert. So, the effective laser flux power has been calibrated using a simple (3-s) laser heating cycle of the insert alone (Fig. 2c) and the matching numerical calculation. The aim is to adjust numerically the value of the heating flux in order to fit temperature measurements of thermocouples 1, 2 and 3 with corresponding computed results.

In this configuration, only the convection heat transfer with the air is considered (the insert is set on three ceramic picks, Fig. 2c). To justify this assumption, it is possible to estimate an order of magnitude of the power transferred by radiation. The Equation (3) is considered:

$$P_{\text{rad}} = \varepsilon \cdot \sigma \cdot A \cdot T^4 \tag{3}$$

where P_{rad} is the power transferred by radiation in W, ε is the emissivity factor (considered as equal to 1 for this estimate), σ is the Stefan–Boltzmann constant ($\sigma = 5.670 \times 10^{-8}$ W m^{-2} K^{-4}), A is the surface area and T is the absolute temperature.

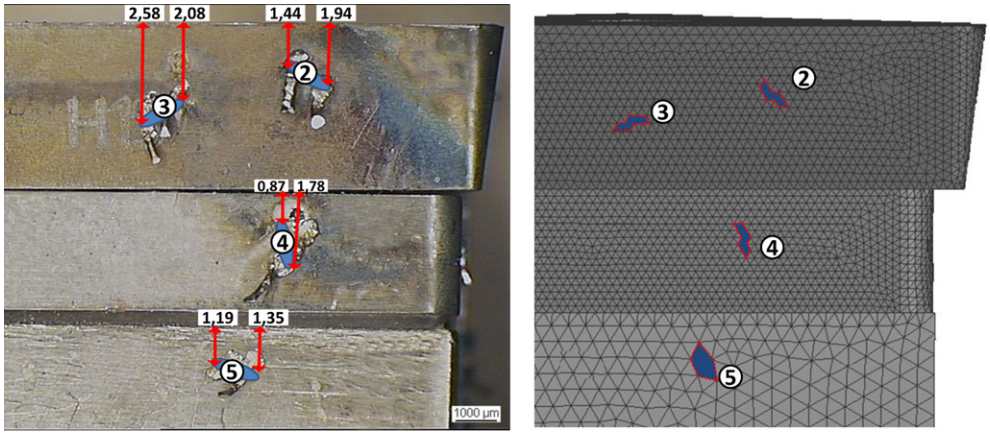

Fig. 4. Example of correspondence between thermocouple locations and set of nodes used to extract temperature results.

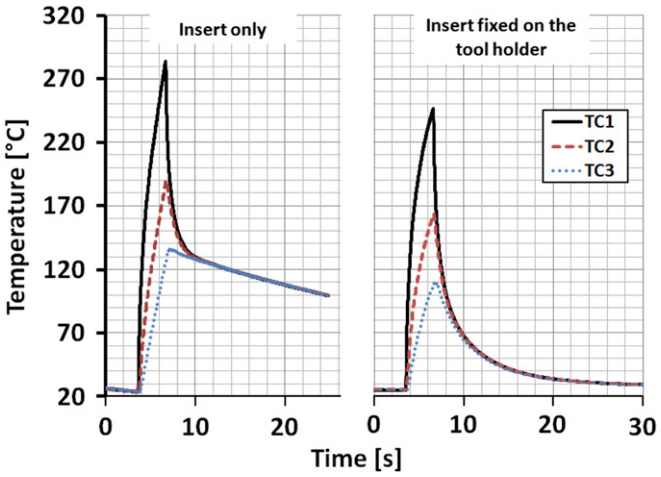

Fig. 6. Comparison of the heating and cooling curves of the insert alone and the "insert + tool-holder" set.

The power transferred by radiation in the laser heating zone ($A = 2 \times 10^{-6}$ m^2 and $T_{average} = 673$ K) could be estimated at $P_{rad} = 0.02$ W and the thermal radiation power for the entire insert surface ($A = 3.5 \times 10^{-4}$ m^2 and $T_{average} = 423$ K) could be estimated at $P_{rad} = 0.6$ W. Due to these small values, the radiation transfer contribution has been neglected in this study. So the convection is the only considered mode of heat transfer. Consequently, the influence of the heat transfer coefficient value h used in the simulation on temperature predictions (and thus indirectly on calibrated values) should be investigated. Fig. 7 presents numerical temperature predictions and comparison with experimental measurement considering the thermocouple 1 during a 3-s laser heating cycle of the insert alone. The sensitivity of the model to the convective heat transfer coefficient value has been tested varying its value of ±20%. Results show that a variation of ±20% of h value has a negligible impact on predicted temperatures during the heating phase (less than 1 °C) or during the beginning of the cooling phase. So, the influence of h value on laser flux power calibration (which is mainly based on the heating phase) is low. Then, the reference h value ($h = 40.10^{-6}$ W/mm^2/°C) has been chosen (Fig. 7) in order to match the experimental temperature measurement to numerical prediction during the end of the cooling phase.

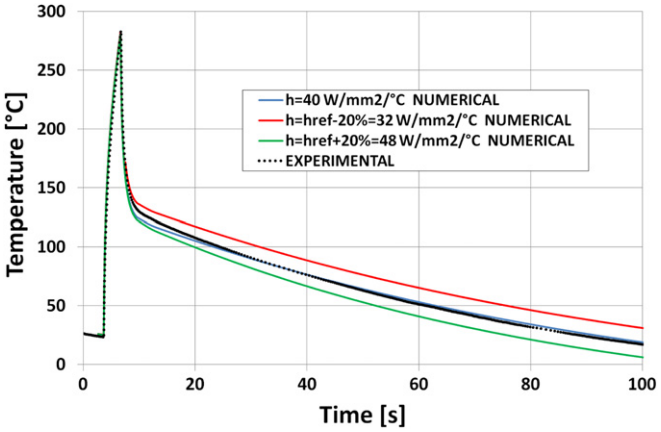

Fig. 7. Comparison between numerical temperature predictions for different value of the convective heat transfer coefficient h and experimental measurement.

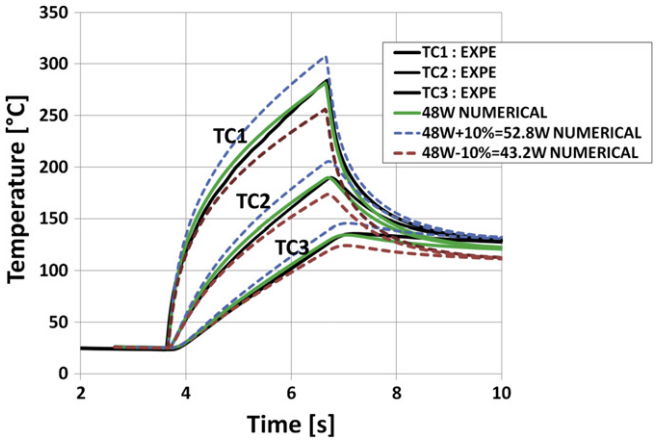

Fig. 8. Calibration of the actual laser heating power.

Finally, the best agreement between experimental and numerical results is obtained when applying a heating flux of 48 W (Fig. 8). The difference between the measured and computed temperatures does not exceed 8 °C. So, compared with the nominal laser power of 70 W, only 68.5% of the power is actually used for the heating of the insert.

The sensitivity of the model to the heat flux value has been tested varying its value of ±10%. A variation of ±10% of the heating power leads to a difference of more than 50 °C between numerical and experimental results after only three seconds of heating (Fig. 8).

4.3. Calibration of the thermal contact resistance between the insert and the tool-holder

During this calibration second step, the aim is to estimate the value of the thermal contact resistance between the insert and the rest of the turning device (shim and tool-holder). As has been previously explained, the shim is stuck on the tool-holder steel body using heat conductive metallic glue. So a perfect thermal contact resistance is assumed between these two parts. The study only focuses on the thermal contact resistance around the insert.

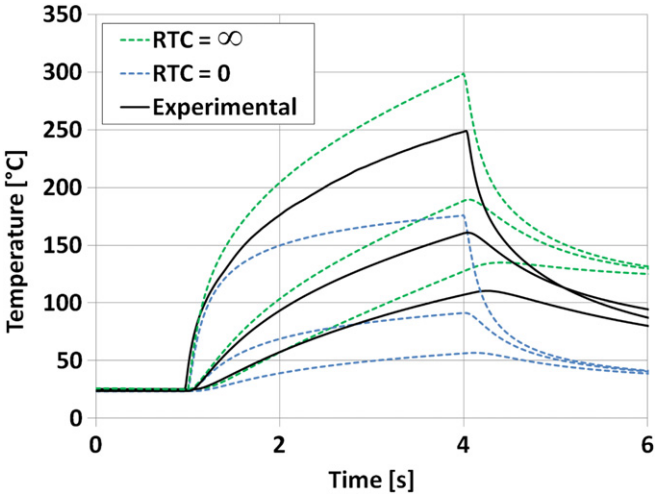

Fig. 9. Comparison between experimental results of temperature measurement and simulation with an infinite and a null thermal contact resistance around the insert.

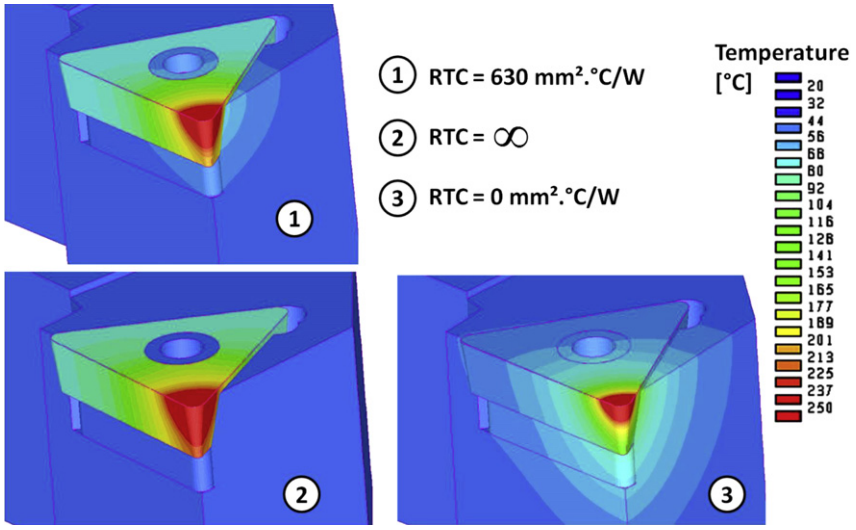

Fig. 10. Comparison between numerically predicted temperature fields for different values of thermal contact resistance around the insert.

The laser heating configuration is exactly the same as in the first calibration step (previously described). The only difference is that the insert is mounted on the tool-holder. So the calibrated value of the heat flux power (48 W) is still suitable.

In the numerical model, the conduction heat transfer is considered between the insert and the rest of the tool-holder. The convection heat transfer with the air is still modeled.

Firstly, Fig. 9 shows the comparison between experimental temperature measurements of thermocouples 1, 2 and 3 (fixed on the insert) and numerical calculations for two configurations:

- a perfect thermal contact around the insert RTC = 0 mm^2 °C/W
- the insert is nearly thermally insulated RTC = 10^6 mm^2 °C/W

The two configurations presented in Figs. 9 and 10 are totally different from experimental results. The temperature difference after only three seconds of heating is more than 50 °C. It clearly shows that, for a stationary machining simulation, the tool cannot be represented by an infinite volume (the heat conduction would be overvalued), nor by the insert alone (the heat conduction would be undervalued). The thermal contact resistance around the insert should be correctly estimated and considered.

Thus, secondly, the value of the thermal contact resistance around the insert has been calibrated to fit experimental and numerical temperature results.

In order to optimize the calibrated RTC value, the deviations between numerical results and experimental temperatures has been studied. Results of the thermocouple 1 during the heating phase (three seconds) and the beginning of the cooling phase (three seconds during which the influence of the RTC prevails) have been considered using the following Equation (4):

$$\mathrm{Dev} = \frac{1}{6s} \cdot \int_{t=0}^{6s} \left[\sqrt{\left(T_{\mathrm{exp}_t} - T_{\mathrm{num}_t}\right)^2} \right] \mathrm{d}t \tag{4}$$

where Dev is the optimization parameter (deviation between experimental and numerical results), T_{exp_t} is the measured experimental temperature at sample time t, T_{num_t} is the predicted numerical temperature at time t. Fig. 11 shows that the Dev parameter clearly reaches a minimum value (representing the best agreement between experimental and numerical results). The thermocouple 1

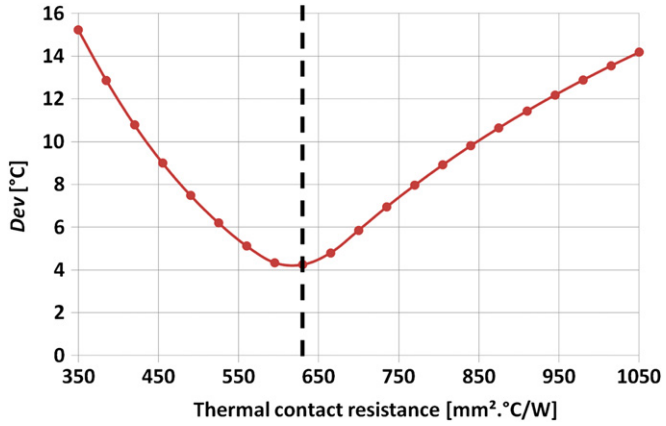

Fig. 11. The deviation parameter (Dev) calculated between numerical and experimental temperature results as a function of the thermal contact resistance value.

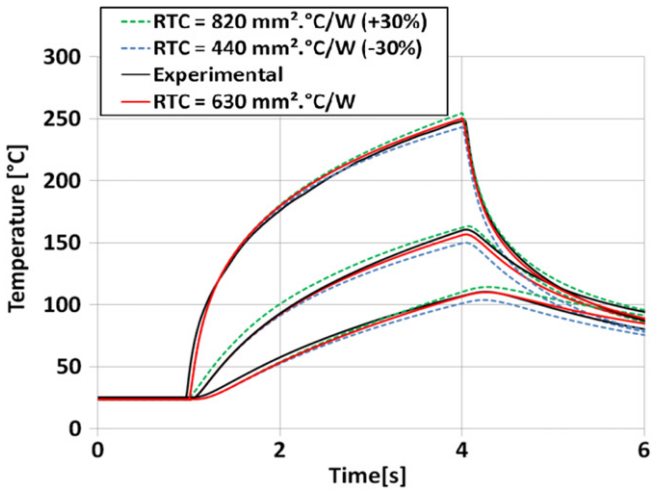

Fig. 12. Comparison between experimental results of temperature measurements and simulation with different values of the thermal contact resistance around the insert.

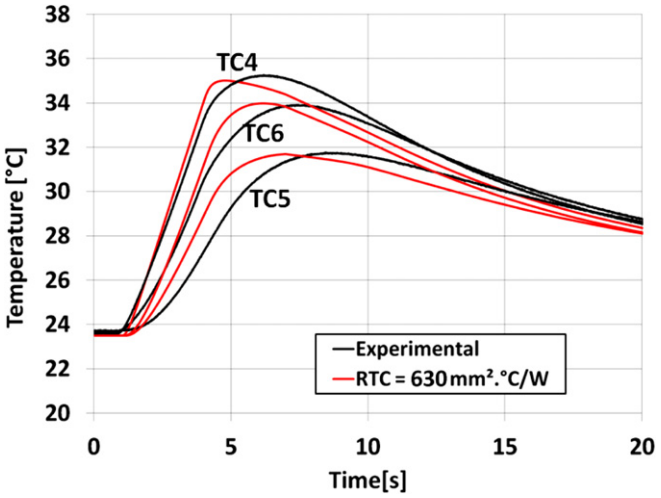

Fig. 13. Comparison between experimental results of temperature measurements and simulation at the insert and tool-holder level.

has been considered since it is the closest to the heating zone. The optimization results are identical regardless of the thermocouple considered.

The retained value is RTC = 630 mm^2 °C/W (Fig. 11). Fig. 12 presents temperature curves computed with RTC = 630 mm^2 °C/W; RTC = 440 mm^2 °C/W (630 − 30%); RTC = 820 mm^2 °C/W (630 + 30%) and a comparison with experimental measurements.

Fig. 13 presented the comparison of numerical and experimental temperature curves for thermocouples fixed on the shim and on the tool-holder (thermocouples 4, 5 and 6). The measured temperatures are clearly below the temperature reached by the insert. Numerical results are obtained with a thermal contact resistance of 630 mm^2 °C/W around the insert and are well matched with experiments. The maximal temperature difference is about 1 °C.

5. Application to other heating cycles

The second calibration step has permitted to approximate the value of the thermal contact resistance around the insert (RTC = 630 mm^2 °C/W). To validate this estimated value, it is important to test this result with other thermal conditions of temperature and heating rate. So, using the same laser heating configuration (the effective heat flux is fixed at 48 W), two other

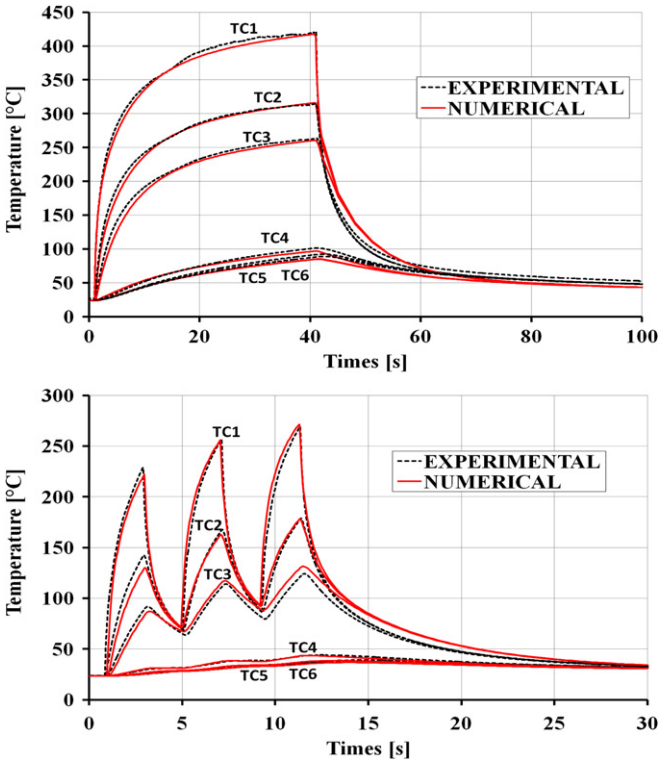

Fig. 15. Comparison between experimental results of temperature measurements and simulation for different thermal cycles.

thermal cycles have been applied experimentally and reproduced numerically. The first one (Fig. 14a) represents a heating phase over a long period of time. The heating phase is forty seconds long, and then the cooling is free. The temperature reached by the insert (thermocouple 1) is high: 425 °C.

The second thermal cycle represents a pulsated heating cycle (Fig. 14b). The heating cycle is composed of three heating phases of two seconds divided by two seconds of free cooling. The importance of the cooling phases is highlighted.

Fig. 15 shows that the results calibrated in the first part of the article can be transferred under different thermal conditions (in terms of temperature range and cycle type). It is to be noted that the experimental results are well matched by the simulation thermal results. The differences are below ten degrees or so.

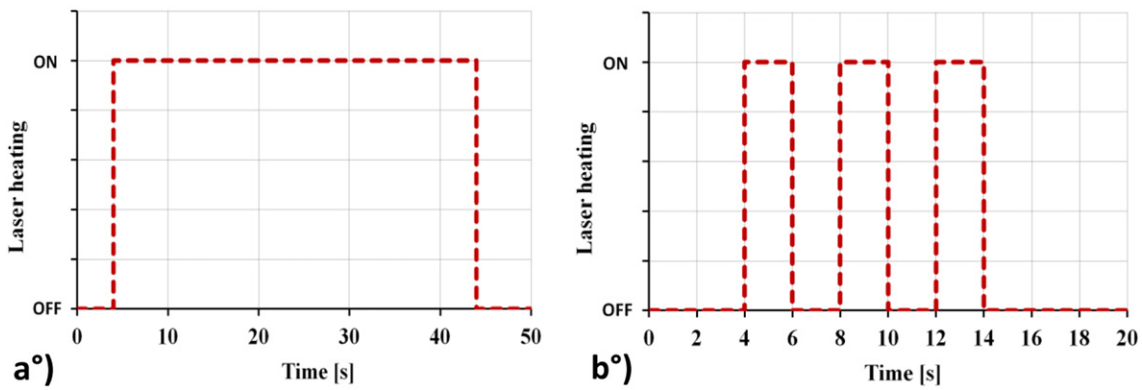

Fig. 14. Tested heating cycle to validate the calibrated value of the thermal contact resistance.

6. Discussion/conclusion

In order to calibrate the thermal aspect of machining simulations, this study has made it possible to provide a bounded value of the thermal contact resistance to apply between the tool and the body. The resistance calibration has been performed in two steps: defining the laser flux power involved in the heating of the insert then defining the thermal resistance value. The value of 630 mm^2 °C/W has been calibrated. Among other things, it is to be noted that, through the study of sensitivity to this resistance value, simulations over long periods of time (or even one second long) taking into consideration a null contact resistance (the tool being represented by an infinite volume) or an infinite one (the tool being represented by the insert alone) would lead to very significant temperature errors. The RTC value determined makes it possible to remove the heat generated by machining under conditions consistent with the reality whatever the thermal cycle applied (pulsed or over a long period of time). Thus this result can be used to simulate a machining operation over a significant period of time (several minutes) and therefore a stabilized thermal state.

References

[1] M.B. da Silva, J. Wallbank, Cutting temperature: prediction and measurement methods-a review, J. Mater. Process. Technol. 88 (1999) 195–202.
[2] E.M. Trent, P.K. Wright, Metal Cutting, fourth ed., Butterworth–Heinemann, Boston, USA, 2000.
[3] F. Valiorgue, J. Rech, H. Hamdi, P. Gilles, J.M. Bergheau, 3D modeling of residual stresses induced in finish turning of an AISI304L stainless steel, Int. J. Mach. Tools Manuf. 53 (2012) 77–90.
[4] Y.C. Yen, J. Sohner, H. Weule, J. Schmidt, T. Altan, Estimation of tool wear of carbide tool in orthogonal cutting using FEM simulation, Mach. Sci. Technol. 6 (2002) 467–486.
[5] A. Mondelin, F. Valiorgue, J. Rech, M. Coret, F. Feulvarch, Numerical prediction of residual stresses in turning of 15-5PH, Adv. Mater. Res. 223 (2011) 411–420.
[6] G. Boothroyd, Photographic technique for the determination of metal cutting temperatures, Br. J. Appl. Phys. 12 (1961) 309–324.
[7] B.T. Chao, H.L. Li, K.J. Trigger, An experimental investigation of temperature distribution at tool-flank surface, Trans. ASME 83 (1961) 496–504.
[8] O.D. Prins, The influence of wear on the temperature distribution at the rake face, Ann. CIRP XVIV (1971) 579–584.
[9] A. Basti, Tools with built-in thin film thermocouple sensors for monitoring cutting temperature, Int. J. Mach. Tools Manuf. 47 (2007) 793–798.
[10] G. Le Coz, M. Marinescu, A. Devillez, D. Dudzinski, L. Velnom, Measuring temperature of rotating cutting tools: application to MQL drilling and dry milling of aerospace alloys, Appl. Therm. Eng. 36 (2012) 434–441.
[11] P. Muller-Hummen, M. Larhes, J. Mehlhose, G. Lang, Measurement of temperature in diamond coated tools during machining processes, Diam. Films Technol. 7 (1997) 219–239.
[12] R. M'Saoubi, C. La Calvez, B. Changeaux, J.L. Lebrun, Thermal and microstructural analysis of orthogonal cutting of a low alloyed carbon steel using an infrared-charge-coupled device camera technique, Proc. Inst. Mech. Eng. 216 (2002) 153–165.
[13] V.M. Luchesi, R.T. Coelho, An inverse method to estimate the moving heat source in machining process, Appl. Therm. Eng. 45–46 (2012) 64–78.
[14] A.J. Shih, H.T.Y. Yang, Experimental and finite element predictions of residual stresses due to orthogonal metal cutting, Int. J. Numer. Methods Eng. 36 (1993) 1487–1507.
[15] Y.K. Potdar, A.T. Zehnder, Measurements and simulations of temperature and deformation fields in transient metal cutting, J. Manuf. Sci. Eng. 125 (2003) 645–655.
[16] M. Barge, H. Hamdi, J. Rech, J.-M. Bergheau, Numerical modelling of orthogonal cutting: influence of numerical parameters, J. Mater. Process. Technol. 164–165 (2005) 1148–1153.
[17] R. Rakotomalala, Arbitrary Lagrangian–Eulerian thermomechanical finite-element model of material cutting, Commun. Numer. Methods Eng. 9 (1993) 975–987.
[18] M.N.A. Nasr, E.G. Ng, M.A. Elbestawi, Modelling the effects of tool-edge radius on residual stresses when orthogonal cutting AISI 316L, Int. J. Mach. Tools Manuf. 47 (2007) 401–411.
[19] C. Bonnet, F. Valiorgue, J. Rech, H. Hamdi, Improvement of the numerical modeling in orthogonal dry cutting of an AISI 316L stainless steel by the introduction of a new friction model, CIRP J. Manuf. Sci. Technol. 1 (2008) 114–118.
[20] L.J. Xie, J. Schmidta, C. Schmidta, F. Biesingerb, 2D FEM estimate of tool wear in turning operation, Wear 258 (2005) 1479–1490.
[21] W. Grzesik, Advanced Machining Processes of Metallic Materials, Elsevier Science, 2008.
[22] C. Courbon, T. Mabrouki, J. Rech, D. Mazuyer, E. D'Eramo, On the existence of a thermal contact resistance at the tool-chip interface in dry cutting of AISI 1045: formation mechanisms and influence on the cutting process, Appl. Therm. Eng. 50 (2013) 1311–1325.
[23] B. Bourouga, V. Goizet, J.P. Bardon, Predictive model of dynamic thermal contact resistance adapted to the case of the interface part-forging tool, Int. J. Heat Mass. Transf. 46 (2003) 565–576 (in French).
[24] B. Abdulhay, B. Bourouga, C. Dessain, Experimental and theoretical study of thermal aspects of the hot stamping process, Appl. Therm. Eng. 31 (2011) 674–685.
[25] B. Abdul Hay, B. Bourouga, C. Dessain, Thermal contact resistance estimation at the blank/tool interface: experimental approach to simulate the blank cooling during the hot stamping process, Int. J. Mater. Form. 3 (2010) 147–163.
[26] P. Rogeon, P. Carre, J. Costa, G. Sibilia, G. Saindrenan, Characterization of electrical contact conditions in spot welding assemblies, J. Mater. Process. Technol. 195 (2008) 117–124.
[27] M. Rosochowska, R. Balendra, K. Chodnikiewicz, Measurements of thermal contact conductance, J. Mater. Process. Technol. 135 (2003) 204–210.
[28] N.A. Abukhshim, P.T. Mativenga, M.A. Sheikh, Investigation of heat partition in high speed turning of high strength alloy steel, Int. J. Mach. Tools Manuf. 45 (2005) 1687–1695.
[29] S.R. Carvalho, S.M.M. Lima e Silva, A.R. Machado, G. Guimaraes, Temperature determination at the chip–tool interface using an inverse thermal model considering the tool and tool-holder, J. Mater. Process. Technol. 179 (2006) 97–104.
[30] E. Feulvarch, J.M. Bergheau, J.B. Leblond, An implicit finite element algorithm for the simulation of diffusion with phase changes in solids, Int. J. Numer. Methods Eng. 78 (2009) 1492–1512.
[31] Z.Y. Wang, K.P. Rajurkar, Cryogenic machining of hard-to-cut materials, Wear 239 (2000) 168–175.
[32] Sandvik Coromant, unpublished internal report, Carbide comparison H13A-HM-H10F, 2009.
[33] ThyssenKrupp Materials, www.onlinemetals.com (accessed 06.02.13).
[34] J.F. Remacle, Difi/Research Fund for Coal and Steel, www.infosteel.be/difisekPlus/04_Partie2_Transfert_thermique_JFR.pdf (accessed 06.02.13).